REVIEW ARTICLE

A review on material models for isotropic hyperelasticity

Stephen K. Melly[1] | Liwu Liu[1] | Yanju Liu[1] | Jinsong Leng[2]

[1]Department of Astronautical Science and Mechanics, Harbin Institute of Technology (HIT), Harbin, China

[2]Center for Composite Materials and Structures, Harbin Institute of Technology (HIT), Harbin, China

Correspondence
Prof. Liwu Liu, Department of Astronautical Science and Mechanics, Harbin Institute of Technology (HIT), P.O. Box 301, No. 92 West Dazhi St., Harbin 150001, China.
Email: liuliwu_006@163.com

Abstract

Dozens of hyperelastic models have been formulated and have been extremely handy in understanding the complex mechanical behavior of materials that exhibit hyperelastic behavior (characterized by large nonlinear elastic deformations that are completely recoverable) such as elastomers, polymers, and even biological tissues. These models are indispensable in the design of complex engineering components such as engine mounts and structural bearings in the automotive and aerospace industries and vibration isolators and shock absorbers in mechanical systems. Particularly, the problem of vibration control in mechanical system dynamics is extremely important and, therefore, knowledge of accurate hyperelastic models facilitates optimum designs and the development of three-dimensional finite element system dynamics for studying the large and nonlinear deformation behavior. This review work intends to enhance the knowledge of 15 of the most commonly used hyperelastic models and consequently help design engineers and scientists make informed decisions on the right ones to use. For each of the models, expressions for the strain-energy function and the Cauchy stress for both arbitrary loading assuming compressibility and each of the three loading modes (uniaxial tension, equibiaxial tension, and pure shear) assuming incompressibility are provided. Furthermore, the stress–strain or stress–stretch plots of the model's predictions in each of the loading modes are compared with that of the classical experimental data of Treloar and the coefficient of determination is utilized as a measure of the model's predictive ability. Lastly, a ranking scheme is proposed based on the model's ability to predict each of the loading modes with minimum deviations and the overall coefficient of determination.

KEYWORDS
constitutive models, finite deformation, hyperelastic, mechanical system dynamics, strain energy density

1 | INTRODUCTION

Elastomers (derived from elastic polymers) are polymeric materials that exhibit both viscous and elastic behavior. Characteristics of these materials, which are also known as rubber-like materials as they exhibit rubber-like properties, include high reversible deformations (up to 500% strains) without fracture, high damping properties, low thermal and electrical conductivity, durability, and hysteresis under cyclic loading.[1] The most important property is its large nonlinear elastic deformation leading to their categorization as hyperelastic/green elastic materials. These properties are highly desirable in a myriad of engineering applications such as engine mountings, structural bearings, vibration absorbers, corrosion protection, tires, medical devices, shock isolators, and springs.[1,2] Due to their extensive applicability, rubber-like materials have attracted huge research interests over the years. The main objective is to understand their stress–strain or stress–stretch behavior under different loading scenarios to aid in the design of complex devices and predict their mechanical behavior during service. The development of what is now robust research in the mechanics of hyperelastic materials began in the early 1940s when Mooney,[3] through his uniaxial tension experiments on soft rubber materials, noted that neither the force-elongation nor the stress–stretch response of the material agreed with Hook's law. It was, therefore, concluded that Hook's law is inadequate in approximating the stress–strain behavior of elastomeric materials. This led to the formulation of the nonlinear theory of elasticity which stemmed out from the classical elasticity theory to accommodate for the large strain nonlinear response of elastomeric materials.

Both hyperelasticity and linear elasticity are reversible processes (no internal energy dissipation) meaning that the work done during the loading process is completely recovered when the load is removed. The difference is that for hyperelastic materials, the deformation can be extremely large and the relationship between the stress and strain is nonlinear. Derivation of the stress–strain relationship for the hyperelastic materials is based on a function known as Helmholtz free energy per unit reference volume (Ψ).[4] It is also known as strain energy density, strain energy function, or the elastic potential and is a scalar-valued function that relates the strain energy to the state of deformation. The unique trait of hyperelastic materials is that the strain energy density is dependent only on the current strain and not on the loading history.[5] The formulation of hyperelastic material models begins with the development of a suitable strain energy density function. Several assumptions are adhered to in deducing the strain energy function. These include that the material is isotropic, homogenous, free of hysteresis, strain-rate independent, and nearly or purely incompressible.[6] Furthermore, various restrictions on the strain energy density such as being nonnegative, having a zero value at undeformed state, and being invariant under coordinate transformations have been proposed by several texts.[7] Over the years, dozens of constitutive models for hyperelastic materials have been formulated by various research groups. Based on the approach with which the models are formulated, they can be categorized as either phenomenological or micromechanical. As the name suggests, phenomenological-based models arise from the observation of rubber-like materials under different conditions of homogenous deformation and thereafter fitting mathematical equations to the experimental data.[8] These equations result in polynomial formulations which further classify the phenomenological models into subcategories based on strain invariants, principal stretches, or a combination of both. On the other hand, the micromechanical models exploit the techniques of statistical mechanics to describe the behavior of hyperelastic materials at the microscopic and macroscopic levels. Even though the phenomenological models make up a larger percentage of the hyperelastic models in the literature, micromechanical-based models have got more attention thanks to their governing parameters that can relate the mechanical behavior with the physical or chemical structure of the material.[9]

Apart from the synthesis of new hyperelastic materials that require new constitutive relations to predict their mechanical behavior, formulating models that accurately describe the complete behavior of the material remains the main motivating factor to researchers. By *complete behavior*, we mean the capability of the model to predict the behavior under uniaxial extension, biaxial extension, and pure shear.[10] Treloar in his paper,[11] provided the experimental data that has been the main reference for researchers in testing new models and their predictive abilities in all three modes of loading. The challenges involving the material models include their predictive ability and the number of parameters required. Most models may predict the behavior in one mode of loading such as the uniaxial extension to good accuracy and fail in the other two modes. Again, some models require many material parameters that may be difficult or time-consuming to achieve through experimental means. It is desirable to have a model that can reproduce experimental data in all the loading modes and has the least number of parameters that are easy to obtain experimentally. Choosing a model for a specific application is determined by several factors such as its accuracy, available or achievable parameters, ease of implementation, material type, loading type, and so on.

It is worth noting that most of the new model developments are modified versions of the already established models to improve their predictive abilities. For instance, Arruda-Boyce's eight-chain (EC) model[12] which is micromechanically inspired and one of the most accurate models, is known to be relatively inaccurate in predicting the behavior during biaxial extension loading. As such, several modified versions of the EC model have been reported in the literature some of which were subjected to a comparative study by Hossain et al.[13] where they found that the bootstrapped EC model by Miroshnychenko and Green[14] performed better than the classical EC model. Recently, Melly et al.[15] modified the strain energy density function expression of Carroll's model[16] to comply with the restriction that it should yield a zero value at the undeformed state and to account for the volume changes during deformation. Their numerical computations demonstrated the relative advantages of the modified version which include superior predictive capabilities in the equibiaxial loading, a single fitting process for model constants (the original version requires three steps), and implementable in a finite

—WILEY—

element program. Anssari-Benam and Bucchi[17] proposed a generalized neo-Hookean type model with only two parameters that have a physical meaning. With a single set of parameters, the model was demonstrated to accurately describe the deformation behavior of several elastomeric materials in uniaxial, equibiaxial, and pure shear loading modes. With the increasing number of models, a comparison between their performances in reproducing different loading conditions based on the classical experimental data by Treloar[11] has been the focus of some review works in literature. For instance, Martins et al.[18] undertook a comparative study on seven hyperelastic models focusing on their ability to reproduce the behavior of silicone rubber and soft tissues. They reported Martin's model[19] to have a very good fit for the materials tested. Other noteworthy review works are those of Steinmann et al.[9] and Sweeney[20] who compared the performance of 14 and 3 hyperelastic models, respectively.

Indeed, the ubiquity of rubber-like materials and their vast applications especially for engineering purposes, for example, aerospace components where their mechanical behavior plays a crucial role in service has made the research on their mechanics one of the most active research at the moment. Obtaining constitutive relations of hyperelastic materials that can predict the behavior in different loading conditions can significantly expedite the design process and ensure structure reliability during service. Numerical simulation has become an indispensable part of the design process thanks to the advances in computing capabilities of modern computers and finite element codes. With dozens of models in the literature, it is imperative to the design engineers to understand the type of models to utilize in their simulations depending on the material type, accuracy, loading type, computational cost, availability of parameters, and so on. A review of the models provides the engineers and upcoming researchers the opportunity to hasten their understanding of the same. There have been remarkable reviews in the literature about constitutive models for rubber-like materials. One of the most referenced reviews on rubber elasticity models was authored by Boyce and Arruda[21] more than two decades ago. They reviewed a total of 11 rubber elasticity constitutive models that are formulated based on both the statistical mechanics and invariant or stretch-based continuum mechanics theories. Importantly, they included a discussion on two common approaches of modeling the compressibility of elastomers. Another frequently cited review work on hyperelastic models was authored by Marckmann and Verron[10] in the year 2006 in which they compared the performance of 20 hyperelastic models based on their ability to reproduce experimental data in different types of loading conditions for two sets of classical experimental data. Moreover, they proposed a ranking scheme to list the models from the best to the worst based on a number of indicators namely the capability of the model to achieve complete behavior, the number of required material parameters, the ability of the model to reproduce both sets of experimental data with the same set of parameters, and whether the parameters are physically motivated. Models which could reproduce experimental behavior in different loading conditions, required few parameters, reproduced both sets of data without changing parameters, and whose parameters have physical meaning were highly ranked. In 2019, Dal et al.[22] presented a comparative study of 40 hyperelastic

models while focusing on the parameter identification process. They proposed a novel parameter identification toolbox based on a multi-objective optimization technique that selects the best model and its parameters from an input of uniaxial tension, equibiaxial extension, and pure shear experimental data. The models were then ranked based on the quality of fit for simultaneous fits for two sets of experimental data. Most recently, Dal et al.[23] extended the previously mentioned work into a comprehensive state of the art involving 44 hyperelastic models. The ranking of the models was not only based on the quality of fit for simultaneous fits but also the number of material parameters and the validity range.

Considering the growing interest in hyperelastic materials and the role played by numerical simulation in product design, this review work aims to bring about the knowledge of the most commonly utilized material models for hyperelastic materials concisely for the benefit of design engineers and researchers. In this study, while presenting our discussions, we classify the models into the two mentioned main categories namely phenomenological and micromechanical where the former is further subdivided into those based on invariants or principal stretches. The discussion on each model mainly focuses on the strain energy density expression, nominal stress–strain or stress–stretch expressions for arbitrary or specific loading conditions (uniaxial tension, equibiaxial extension, or pure shear), material parameters, and their predictive capabilities according to Treloar's data. Illustrations that compare the experimental and the predicted stress–strain or stress–stretch curves are presented and the accuracy is quantified using the coefficient of determination. Importantly, this study proposes a novel ranking scheme that considers the behavior of the model in each loading mode, the overall behavior, and the deviation of the fitness coefficient for each loading mode in the experimental data set.

2 | PHENOMENOLOGICAL MODELS

Constitutive models emanating from the phenomenological approach are formulated by fitting mathematical equations to the experimentally observed behavior of the material.[24] The formulation considers the macroscopic nature of the material hence treating the problem from the continuum mechanics viewpoint.[25] There are two categories of phenomenological constitutive models; those that are based on the invariants of the Cauchy–Green deformation tensors as introduced by Rivlin[26] and those based on the principle stretches as introduced by Valanis and Landel[27] and Ogden.[28] In this section, we present the mentioned categories of phenomenological models while giving the most common examples of each. Readers interested in comprehensive coverage of phenomenological models may refer to the work of Vahapoğlu and Karadeniz[24] and Beda.[29] It is worth noting that most of the models were originally formulated with an assumption of incompressibility. As put by Boyce and Arruda,[21] the mentioned assumption has the advantage of simplifying the model equations and achieves acceptable accuracy but does not represent

the real behavior of elastomeric materials. Practically, these materials undergo volume changes, especially when subjected to hydrostatic deformations. Consequently, the most accurate constitutive models must account for compressibility. Not only is it important for accuracy but also for avoiding numerical problems during finite element implementation of the model. To include a compressibility term, the Ψ expression is additively decomposed into volumetric and deviatoric parts which are responsible for volume and shape changes respectively as shown in Equation (1).

$$\Psi = \Psi_d(I_1^*, I_2^*) + \Psi_v(J), \tag{1}$$

where the subscripts d and v represent the deviatoric and volumetric parts respectively. J is the volume ratio and is obtained by the determinant of the deformation gradient $J = \det\mathbf{F}$ whereas I_1^* and I_2^* are the distortional parts of the first and the second invariants of Cauchy–Green deformation tensors and are obtained as shown in Equation (2).

$$I_1^* = J^{-2/3}I_1, \; I_2^* = J^{-4/3}I_2 \tag{2}$$

This study utilizes the most commonly used expression for the volumetric part according to[30] and is given by $\Psi_v = 0.5K(J-1)^2$ where K is the bulk modulus of the material.

2.1 | Invariants based

2.1.1 | Neo-Hookean (NH)

It was firstly formulated by the renowned rubber expert, Ronald Rivlin, in 1948. It is an extension of Hook's law for linear elasticity to include large deformations where the stress–strain relationship is nonlinear. It is the most commonly used and well-known hyperelastic model due to its simplicity as it requires only two material parameters that can be easily determined; the shear modulus (μ) and the bulk modulus (κ). Of the two material parameters, the former controls the deviatoric response whereas the latter controls the volumetric response.[31] If incompressibility is assumed, that is, no volume change during deformation (as is frequently done in theoretical calculations), the expression becomes even simpler as only the shear modulus parameter is required. As with all the hyperelastic constitutive equations, the NH model is derived from its corresponding expression for strain energy density function (Ψ) as shown in Equation (3). It is worth noting that several authors have slightly varying expressions for Ψ. This study is based on the expressions by Bergström.[32]

$$\Psi(I_1^*, J) = \frac{\mu}{2}(I_1^* - 3) + \frac{k}{2}(J-1)^2, \tag{3}$$

The terms in Equation (3) are as follows; μ = shear modulus, $J = \det[\mathbf{F}]$, where $\mathbf{F}$ is the deformation gradient, $I_1^* = tr(\mathbf{C}^*)$, where $\mathbf{C}^* = J^{(-2/3)}\mathbf{C}$ (distortional part of the right Cauchy–Green deformation tensor), k = bulk modulus. By assuming an incompressible

deformation, $J = 1$, thus reducing the energy expression to $\Psi(I_1^*) = \mu/2(I_1^* - 3)$. From the energy expression, the NH model's Cauchy stress for an arbitrary loading mode is obtained as shown in Equation (4).

$$\sigma = \frac{\mu}{J}dev[\mathbf{B}^*] + k(J-1)\mathbf{I}, \tag{4}$$

where $\mathbf{B}^* = J^{(-2/3)}\mathbf{B}$ (distortional part of the left Cauchy–Green deformation tensor). When incompressibility of the material is assumed, the Cauchy stress for the three loading modes; uniaxial, planar, and biaxial are given in Equation (5).

$$\sigma_u = \mu\left(\lambda^2 - \frac{1}{\lambda}\right), \sigma_p = \mu\left(\lambda^2 - \frac{1}{\lambda^2}\right), \sigma_b = \mu\left(\lambda^2 - \frac{1}{\lambda^4}\right), \tag{5}$$

The subscripts u, p, and b represent uniaxial, planar, and biaxial loading respectively whereas λ represent the stretch applied.

The accuracy of the NH model, as with any other hyperelastic model, can be approximated by comparing its stress–strain predictions to that of the classical experimental data by Treloar[11] as shown in Figure 1A. The coefficient of determination (R^2) as shown in Equation (6) is utilized to rate the level of accuracy of the predicted data. While the R^2 is used to indicate the closeness of the predicted data to the experimental data in an individual loading mode, $\bar{R}^2$ indicates the complete behavior of the model and is obtained by a simple average of R^2 in the three loading modes. From Figure 1A, it can be observed that the NH model is suitable for predicting uniaxial tension behavior for up to about 40% strain and planar loading up to about 90% strain. The reason for the low accuracy in high uniaxial strains is because of its linear dependence on I_1^*. Similarly, biaxial loading predictions may be underestimated because the model expression lacks the dependence on the second invariant I_2^* of the deviatoric Cauchy–Green deformation tensor. As put by Bergström,[32] the main advantages of this model include its simplicity and computationally efficient implementation whereas the drawback is its stringent conditions for accuracy.

$$R^2 = 1 - \frac{\sum\limits_{i=1}^{n}(e_i - p_i)^2}{\sum\limits_{i=1}^{n}(e_i - e_m)^2}, \tag{6}$$

where n = number of data points, e_i = experimental data at a point i, p_i = prediction data at a point i, and e_m = the mean of the experimental data.

2.1.2 | Yeoh

While experimenting on the behavior of carbon black reinforced rubber, Yeoh[33,34] observed that the shear modulus significantly dropped at low strains. The available hyperelastic models at that time could not predict
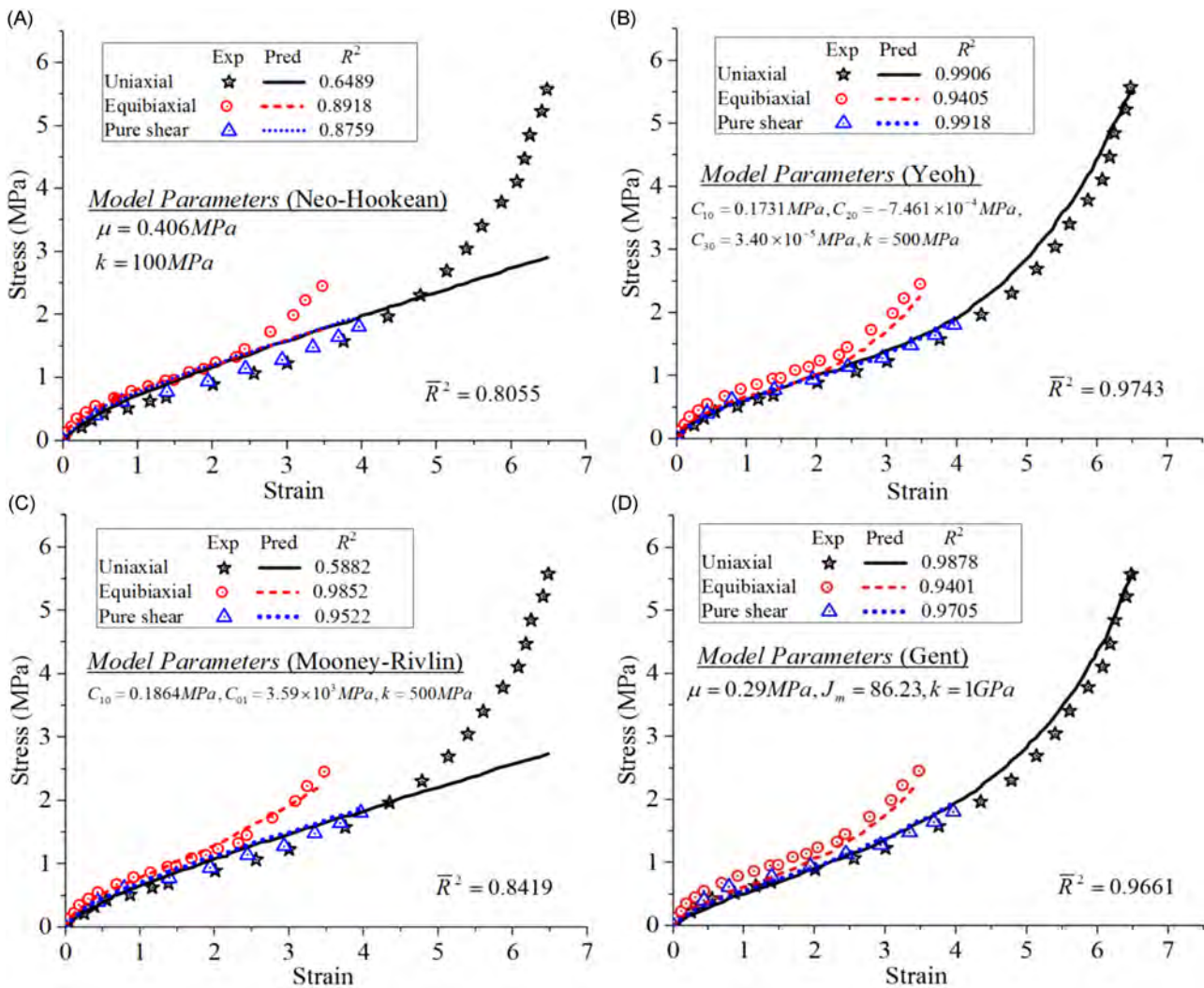
FIGURE 1 Comparisons of the model predictions and the experimental engineering stress-strain curves showing the model parameters and the coefficient of determination for uniaxial, equibiaxial, and planar shear loading modes for models (A) Neo-Hookean, (B) Yeoh, (C) Mooney-Rivlin, and (D) Gent. The predicted and the experimental data were obtained from Bergström[32] and Treloar,[11] respectively

this behavior accurately. He proposed the addition of exponentially decaying terms to the strain energy function resulting in an expression that is a polynomial of I_1^* without the dependence of the second invariant as shown in Equation (7). The work of Kawabata et al.[35] found that the Helmholtz free energy for most rubber-like materials is less dependent on I_2^* than on I_1^*. Furthermore, it is more strenuous to determine by experimental means how I_2^* influences the energy function. This motivated Yeoh to drop the dependence of I_2^* in his expression.

$$\Psi = \sum_{i=1}^{N} C_{i0}(I_1^* - 3)^i + \sum_{m=1}^{N} k_m (J - 1)^{2m}. \quad (7)$$

The terms C_{i0} and k_m in Equation (7) above are the material parameters to be determined whereas N is an input integer representing the order of the polynomial.

If three orders are considered in the strain energy function (hence $N = 3$), the Cauchy stress considering compressibility in arbitrary loading mode as given by Bergström[32] is shown in Equation (8).

$$\sigma = \frac{2}{J}\{C_{10} + 2C_{20}(I_1 - 3) + 3C_{30}(I_1^* - 3)^2\}dev[\mathbf{B}^*] + k(J - 1)\mathbf{I}. \quad (8)$$

On the other hand, Cauchy stress expression when incompressibility is assumed for each of the three loading modes is given in Equation (9).

$$\sigma_u = 2[C_{10} + 2C_{20}(I_1^* - 3) + 3C_{30}(I_1 - 3)^2]\left(\lambda^2 - \frac{1}{\lambda}\right),$$
$$\sigma_p = 2[C_{10} + 2C_{20}(I_1^* - 3) + 3C_{30}(I_1 - 3)^2]\left(\lambda^2 - \frac{1}{\lambda^2}\right), \quad (9)$$
$$\sigma_b = 2[C_{10} + 2C_{20}(I_1^* - 3) + 3C_{30}(I_1 - 3)^2]\left(\lambda^2 - \frac{1}{\lambda^4}\right).$$

It is worth noting that if only the first order is considered, that is, $N = 1$, the expression then becomes equivalent to the NH model. By comparing the Yeoh model predictions to the classical Treloar data as shown in Figure 1B, it is evident that the Yeoh model prediction is to a higher accuracy relative to the NH model in different loading modes. The model has the advantage of being simple (no dependence on the second invariant), few parameters required, and having improved predictive ability.

2.1.3 | Mooney–Rivlin

This model was formulated by Mooney[3] and Rivlin[36] and has a reputation for predicting the response of hyperelastic materials to a high level of accuracy, therefore, it is well known and most commonly preferred model. Such improved accuracy is a result of the inclusion of linear dependence on I_2^* in the strain energy function. This means that the deviatoric response is defined by both the first and the second invariant. One way of expressing the strain energy function is shown in Equation (10).

$$\Psi(C_{10}, C_{01}, k) = C_{10}(I_1^* - 3) + C_{01}(I_2^* - 3) + \frac{k}{2}(J - 1)^2, \quad (10)$$

where C_{10}, C_{01}, and k are the material parameters required for this model whereas $I_2^* = \frac{1}{2}[(tr(\mathbf{C}))^2 - tr(\mathbf{C})^2]$. Considering compressibility during deformation, the Cauchy stress expression for arbitrary loading is obtained as shown in Equation (11).

$$\sigma = \frac{2}{J}(C_{10} + C_{01}I_1^*)\mathbf{B}^* - \frac{2C_{01}}{J}(\mathbf{B}^*)^2 + \left[k(J - 1) - \frac{2I_1^* C_{10}}{3J} - \frac{4I_2^* C_{01}}{3J}\right]\mathbf{I}. \quad (11)$$

The incompressible forms of Cauchy stress for uniaxial, planar, and biaxial loading are given in Equation (12).

$$\begin{aligned}
\sigma_u &= 2\left(\lambda^2 - \frac{1}{\lambda}\right)\left[C_{10} + \frac{C_{01}}{\lambda}\right], \\
\sigma_P &= 2\left(\lambda^2 - \frac{1}{\lambda^2}\right)\left[C_{10} + C_{01}\right], \\
\sigma_b &= 2C_{10}\left(\lambda^2 - \frac{1}{\lambda^4}\right) + 2C_{01}\left(\lambda^4 - \frac{1}{\lambda^2}\right).
\end{aligned} \quad (12)$$

The Mooney–Rivlin model works well from small to medium strains. The plots which are shown in Figure 1C compare the model's stress–strain predictions with the experimental results of Treloar. The model has improved accuracy relative to that of the NH model.

2.1.4 | Gent

The Gent model[37] was formulated based on the NH model with the aim of better characterization of rubberlike materials when subjected to large deformations. The strain energy density function expression for this model is a logarithmic function of I_1^* with three material parameters. In addition to the shear modulus and the bulk modulus as in the NH model, it also has another dimensional parameter denoted as J_m which controls the chain extensibility at large strains. This ensures that the energy density function has a singularity when $I_1^* = J_m$. The original work by Gent assumed incompressibility in formulating the strain energy density expression. The expression shown in Equation (13) has been modified by Bergström[32] to include a compressibility term.

$$\Psi(I_1^*, J) = \frac{-\mu}{2}J_m \ln\left(1 - \frac{I_1^* - 3}{J_m}\right) + \frac{k}{2}[J - 1]^2. \quad (13)$$

The Cauchy stress expression obtained for arbitrary loading and considering compressibility is given in Equation (14)

$$\sigma = \frac{\mu}{J}\frac{1}{1 - \frac{I_1^* - 3}{J_m}}dev[\mathbf{B}^*] + k[J - 1]\mathbf{I}. \quad (14)$$

From Equation (14), it is worth noting that as J_m tends towards positive infinity, the Gent model's Cauchy stress expression becomes equivalent to that of NH. The incompressible forms of Cauchy stresses for the Gent model are given in Equation (15).

$$\begin{aligned}
\sigma_u &= \mu\left(\lambda^2 - \frac{1}{\lambda}\right)\frac{J_m}{J_m - (\lambda^2 + 2/\lambda - 3)}, \\
\sigma_p &= \mu\left(\lambda^2 - \frac{1}{\lambda^2}\right)\frac{J_m}{J_m - (\lambda^2 + 2/\lambda - 3)}, \\
\sigma_b &= \mu\left(\lambda^2 - \frac{1}{\lambda^4}\right)\frac{J_m}{J_m - (\lambda^2 + 2/\lambda - 3)}.
\end{aligned} \quad (15)$$

The Gent model has the advantage of being able to predict large strain loadings (up to 300%), higher accuracy, and also requires only three parameters. As shown in Figure 1D, the Gent model does relatively well in predicting the material behavior and its accuracy is close to that of the Yeoh model.

2.1.5 | Isihara

The model was formulated by Isihara et al.[38] and it is considered as a specialized form of the Mooney–Rivlin model since its strain energy density function (see Equation 16) includes the dependence on the second invariant.

$$\Psi(C_{10}, C_{20}, C_{01}) = C_{10}(I_1^* - 3) + C_{20}(I_1^* - 3)^2 + C_{01}(I_2^* - 3). \quad (16)$$

The material parameters required by the incompressible version are C_{10}, C_{20}, and C_{01}. As per the original work, the uniaxial tension Cauchy stress expression for an incompressible deformation is shown in Equation (17).

$$\sigma_u = C_{10}\left(\lambda - \frac{1}{\lambda^2}\right) + C_{01}\left\{\lambda^3 + \frac{C_{20}}{C_{01}} - \left(1 + \frac{C_{20}}{C_{01}}\right)\frac{1}{\lambda^3}\right\}. \quad (17)$$

The predictive capability of the Isihara model is shown in Figure 2A where it is compared with the classical experimental data. It can be observed that uniaxial tension loading predictions are accurate to moderate stretch values. The model poorly estimates the behavior in biaxial loading mode.
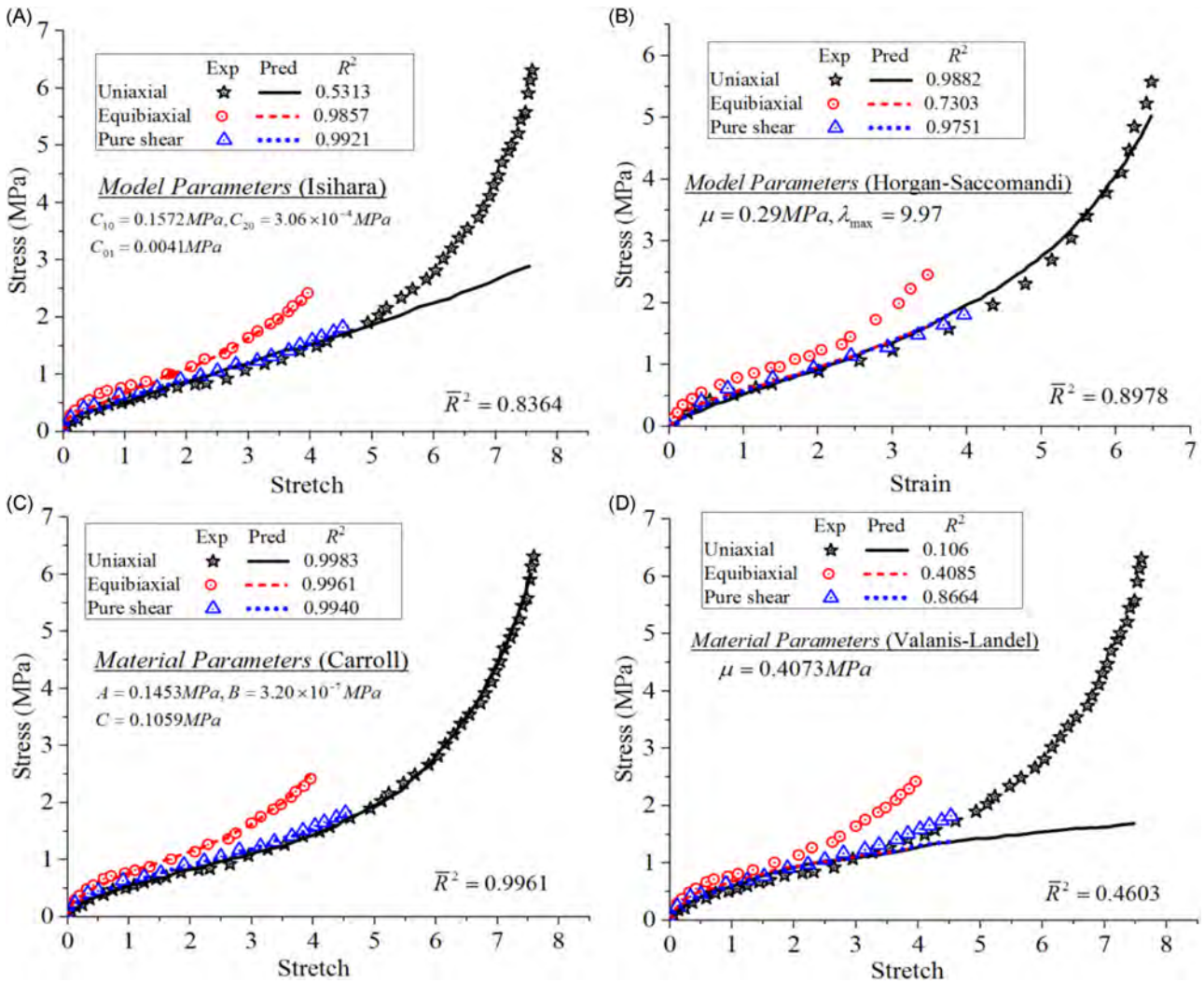
FIGURE 2 Model predictions compared to the experimental data for models (A) Isihara, (B) Horgan-Saccomandi, (C) Carroll, and (D) Valanis-Landel. The stress–stretch prediction data were obtained from Badienia[39]

2.1.6 | Horgan and Saccomandi

The researchers Horgan and Saccomandi[40] aimed to improve the predictive ability of the Gent model by introducing the dependence on I_2^* in the strain energy density function. Their work resulted in a hyperelastic model in their names, Horgan and Saccomandi which we shall shorten to HS for convenience. The difference between the limiting chain stretches in Gent and HS models is that the former depends on the maximum value of the first invariant whereas the latter on the maximum allowable stretch thus more physical significance.[32] Strain energy expression that assumes compressibility for the HS model is given in Equation (18).

$$\Psi(I_1^*, I_2^*, J) = -\frac{\mu}{2}\lambda_{max}^2 \ln\left[\frac{\lambda_{max}^6 - \lambda_{max}^4 I_1^* + \lambda_{max}^2 I_2^* - 1}{(\lambda_{max}^2 - 1)^3}\right] + \frac{k}{2}[J - 1]^2. \quad (18)$$

The parameter λ_{max} represents the limiting chain stretch.

HS's model Cauchy stress expression derived from the strain energy density function is given in Equation (19).

$$\sigma = \frac{\mu\lambda_{max}^4}{J}\frac{\left[\lambda_{max}^2 - I_1^*\right]\mathbf{B}^* + (\mathbf{B}^*) - \frac{1}{3}\left[\lambda_{max}^2 I_1^* - 2I_2^*\right]\mathbf{I}}{\lambda_{max}^6 - \lambda_{max}^4 I_1^* + \lambda_{max}^2 I_2^* - 1} + k[J - 1]\mathbf{I}. \quad (19)$$

As in Gent's model, the HS equates to the NH as the limiting chain stretch approaches infinity. Considering incompressibility, the Cauchy stress for uniaxial tension, planar shear, and equibiaxial tension loading modes are given in Equation (20).

$$\sigma_u = \mu\lambda_{max}^4 \frac{\lambda^3 - 1}{\left(\lambda\lambda_{max}^2 - 1\right)\left(\lambda_{max}^2 - \lambda^2\right)},$$

$$\sigma_p = \mu\lambda_{max}^4 \frac{\lambda^3 - 1}{\left(\lambda^2\lambda_{max}^2 - 1\right)\left(\lambda_{max}^2 - \lambda^2\right)}, \quad (20)$$

$$\sigma_b = \mu\lambda_{max}^4 \frac{\lambda^3 - 1}{\left(\lambda^4\lambda_{max}^2 - 1\right)\left(\lambda_{max}^2 - \lambda^2\right)}.$$

One main advantage of the HS is its stability provided that the shear modulus and limiting chain stretch are greater than zero and one,

respectively. The model's ability to reproduce the experimental material behavior is shown in Figure 2B.

2.1.7 | Carroll model

Carroll[16] undertook a systematic approach considering Treloar's uniaxial and equibiaxial extension data to develop a three-parameter strain energy function. The function is made up of three parts; the first part represents the response of the material in simple extension that is represented accurately by NH strain energy function (according to Treloar's data, up to $\lambda \approx 4.5$), the second and the third parts are the strain energy expressions that model the residual stresses in uniaxial and equibiaxial tension, respectively. The resulting strain energy expression for the Carroll model is shown in Equation (21).

$$\Psi = AI_1 + BI_1^4 + CI_2^{0.5}, \tag{21}$$

where A, B, and C are material parameters found by Carroll to be 0.15, 3.1×10^7, and 0.095, respectively (units = MPa).

According to Steinmann 9, the expressions for the stress–stretch relationship for the three loading modes considering incompressibility are given in Equation (22).

$$\sigma_{UT} = \left[2A + 8B\left[\frac{2}{\lambda} + \lambda^2\right]^3 + C[1 + 2\lambda^3]^{-1/2}\right]\left[\lambda - \frac{1}{\lambda^2}\right],$$

$$\sigma_{EB} = \left[2A + 8B\left[\frac{1}{\lambda^4} + 2\lambda^2\right]^3 + C\lambda^2\left[\frac{2}{\lambda^2} + \lambda^4\right]^{-1/2}\right]\left[\lambda - \frac{1}{\lambda^5}\right], \tag{22}$$

$$\sigma_{PS} = \left[2A + 8B\left[\lambda^2 + \frac{1}{\lambda^2} + 1\right]^3 + C\left[\lambda^2 + \frac{1}{\lambda^2} + 1\right]^{-1/2}\right]\left[\lambda - \frac{1}{\lambda^3}\right].$$

Despite its simplicity, the Carroll model approximates the material response excellently according to Treloar's experimental data as shown in Figure 2C.

2.2 | Stretch based

2.2.1 | Valanis–Landel

To circumvent notable challenges in invariant-based hyperelastic models such as sensitivities to experimental errors at low invariant values (less than five) and difficulties in designing experiments in which the first invariant can be varied while keeping the second constant, Valanis and Landel[27] proposed a strain energy density function while assuming incompressibility that is of the form shown in Equation (23).

$$\Psi(\lambda_1, \lambda_2, \lambda_3) = \psi(\lambda_1) + \psi(\lambda_2) + \psi(\lambda_3), \tag{23}$$

where $\lambda_1, \lambda_2,$ and λ_3 are the principal extension ratios. As in the other hyperelastic materials, the expressions for stress can be obtained by taking the partial derivative of Ψ with respect to $\lambda_i (i = 1, 2, 3)$. Consequently, the components of Cauchy stress in arbitrary loading are given as shown in Equation (24).[41]

$$\sigma_i = I_3^{(-1/2)}\lambda_i \frac{\partial \Psi}{\partial \lambda_i}, \tag{24}$$

where $i = 1, 2, 3$.

The Valanis–Landel model requires only one material parameter for the incompressible form which is the shear modulus. This makes the model simple but reduced accuracy in predicting the material behavior as shown in Figure 2D.

2.2.2 | Ogden

Formulated by Ogden[28] in 1972, it is a versatile hyperelastic model that can describe the mechanical behavior of a wide variety of materials with hyperelastic behavior including polymers and biological matter when subjected to high strains. The energy density function is expressed in principal stretches and there are numerous ways of writing it one of which was done by Bergström[32] as shown in Equation (25).

$$\Psi(\lambda_1^*, \lambda_2^*, \lambda_3^*) = \sum_{k=1}^{N} \frac{2\mu_k}{\alpha_k^2}((\lambda_1^*)^{\alpha_k} + (\lambda_2^*)^{\alpha_k} + (\lambda_3^*)^{\alpha_k} - 3) + \sum_{k=1}^{N} \frac{1}{D_k}(J - 1)^{2k}. \tag{25}$$

The parameters are as follows: N = the order of the model (normally taken as 3), μ_k and α_k^2 are material constants, and D_k is a parameter that indicates volume change. The expression for the principal stresses (σ_i, $i = 1, 2, 3$) is shown in Equation (26).

$$\sigma_i = \frac{2}{J}\sum_{k=1}^{N} \frac{\mu_k}{\alpha_k}\left((\lambda_1^*)^{\alpha_k} - \frac{1}{3}[((\lambda_1^*)^{\alpha_k} + (\lambda_2^*)^{\alpha_k}) + (\lambda_3^*)^{\alpha_k}]\right)$$
$$+ \sum_{k=1}^{N} \frac{2k}{D_k}(J - 1)^{2k-1}. \tag{26}$$

An interesting observation in Equation (26) is that when both N and α_k are equal to 1, then the Ogden model equates to the NH model. Considering incompressibility, the stress expressions for the three loading modes (subscripts $\mu, p,$ and b representing uniaxial, planar, and biaxial loading, respectively) are given in Equation (27).

$$\sigma_u = \sum_{k=1}^{N} \frac{2\mu_k}{\alpha_k}\left[\lambda^{\alpha_k} - \left(\frac{1}{\sqrt{\lambda}}\right)^{\alpha_k}\right],$$

$$\sigma_p = \sum_{k=1}^{N} \frac{2\mu_k}{\alpha_k}\left[\lambda^{\alpha_k} - \left(\frac{1}{\lambda}\right)^{\alpha_k}\right], \tag{27}$$

$$\sigma_b = \sum_{k=1}^{N} \frac{2\mu_k}{\alpha_k}\left[\lambda^{\alpha_k} - \left(\frac{1}{\lambda^2}\right)^{\alpha_k}\right].$$

The predicted stress–stretch response of the Ogden model has been found to agree very well with the classical experimental results of Treloar as shown in Figure 4A. The model is highly suitable for predicting large deformation behavior and can describe well the sharp increase in stiffness at large strains. The main drawback of this model is that material parameters are specific to every deformation mode and, therefore, require different sets of parameters.

2.2.3 | Shariff

In his work, Shariff[42] aimed to overcome the challenge posed by hyperelastic models such as the Ogden model whereby obtaining the material parameters requires the solution of a system of nonlinear equations. He developed an energy function that obeys the Valanis–Landel hypothesis ($\Psi(\lambda_1, \lambda_2, \lambda_3) = \psi(\lambda_1) + \psi(\lambda_2) + \psi(\lambda_3)$) and most importantly being linear in its material parameters as shown in Equation (28).

$$\Psi(\lambda_i) = E \sum_{i=0}^{n} \alpha_i \varphi_i(\lambda_i), \tag{28}$$

where $i = 0, 1, 2, 3, ..., n$, α_i = material parameters, $\alpha_0 = 1$, φ_i = smooth function that takes up to four expansion points as shown in Equation (29) according to Badienia.[39]

$$\varphi(0) = \frac{2\ln(\lambda)}{3}, \qquad \varphi(1) = \exp(1-\lambda) + \lambda - 2,$$

$$\varphi(2) = \exp(\lambda - 1) - \lambda, \qquad \varphi(3) = \frac{(\lambda - 1)^3}{\lambda^{3.6}} \tag{29}$$

To obtain the expressions for the Cauchy stress, the first derivative of Equation (28) with respect to the principle stretch was obtained. The stress expressions for the three loading modes assuming incompressibility according to Hossain and Steinmann[43] are given as shown in Equation (30).

$$\sigma_u = \frac{E}{\lambda}\left[\ln\lambda + \alpha_1\left[e^{1-\lambda} - e^{1-\lambda^{-1/2}} + \lambda - \lambda^{-1/2}\right]\right.$$
$$+ \alpha_2\left[e^{\lambda-1} - e^{\lambda^{-1/2}-1} - \lambda + \lambda^{-1/2}\right] + \alpha_3\left[\frac{[\lambda-1]^3}{\lambda^{3.6}} - \frac{\left[\lambda^{-1/2}-1\right]^3}{\lambda^{-1.8}}\right]$$
$$\left. + \alpha_4\left[[\lambda-1]^3 - \left[\lambda^{-1/2}-1\right]^3\right]\right],$$

$$\sigma_p = \frac{E}{\lambda}\left[\frac{4}{3}\ln\lambda + \alpha_1\left[e^{1-\lambda} - e^{1-\lambda^{-1}} + \lambda - \lambda^{-1}\right]\right.$$
$$+ \alpha_2\left[e^{\lambda-1} - e^{\lambda^{-1}-1} - \lambda + \lambda^{-1}\right] + \alpha_3\left[\frac{[\lambda-1]^3}{\lambda^{3.6}} - \frac{\left[\lambda^{-1}-1\right]^3}{\lambda^{-3.6}}\right]$$
$$\left. + \alpha_4\left[[\lambda-1]^3 - \left[\lambda^{-1}-1\right]^3\right]\right],$$

$$\sigma_b = \frac{E}{\lambda}\left[2\ln\lambda + \alpha_1\left[e^{1-\lambda} - e^{1-\lambda^{-2}} + \lambda - \lambda^{-2}\right]\right.$$
$$+ \alpha_2\left[e^{\lambda-1} - e^{\lambda^{-2}-1} - \lambda + \lambda^{-2}\right] + \alpha_3\left[\frac{[\lambda-1]^3}{\lambda^{3.6}} - \frac{\left[\lambda^{-2}-1\right]^3}{\lambda^{-7.2}}\right]$$
$$\left. + \alpha_4\left[[\lambda-1]^3 - \left[\lambda^{-2}-1\right]^3\right]\right] \tag{30}$$

The Shariff model requires five material parameters which are $E, \alpha_1, \alpha_2, \alpha_3$, and α_4. As shown in Figure 4B, the model accurately captures the observed experimental behavior, particularly, the S-shaped curve behavior at high strains. While extra effort is needed for parameter fitting due to the complexity of the constraint equations, less time is required compared to that of the Ogden model since its energy function is a function of linear parameters.[43]

3 | MICROMECHANICAL MODELS

Micromechanical models arise from analyzing the deformation behavior of rubber-like materials from the microstructural point of view. As it is well known, the microstructure of rubber-like materials consists of randomly oriented long polymeric chains that are joined together into a network structure.[44] Furthermore, the polymeric chains are comprised of N rigid beams which are commonly known as *Kuhn segments* each of equal length l.[39] The ideal maximum length of the chain r_{max} at full elongation is given by $r_{max} = Nl$.[9] Statistical mechanics theory (the random walk theory[45]) is utilized to describe the average end-to-end distance of stress-free undeformed chain which is found as $r = \sqrt{N}l$. The distribution of the end-to-end distance r of a polymeric chain is given by the Gaussian probability distribution function shown in Equation (31).[21]

$$P(r) = 4\pi\left(\frac{3}{2\pi Nl^2}\right)^{3/2} r^2 \exp\left(-\frac{3r^2}{2Nl^2}\right). \tag{31}$$

The Gaussian assumption is only valid for small deformations where the $r \ll Nl$. The stress–stretch response predicted by Gaussian distribution deviates significantly from the observed experimental behavior. As such, non-Gaussian theory is taken into consideration when modeling large deformations where the chain length approaches the full extension length $r/Nl \cong 0.4$. The Langevin function is utilized to account for the finite chain extensibility and the resulting force-extension expression is given in Equation (32).[21]

$$f = \frac{k\theta}{l}\mathcal{L}^{-1}\left(\frac{r}{nl}\right) = \frac{k\theta}{l}\mathcal{L}^{-1}\frac{\lambda}{\sqrt{N}}. \tag{32}$$

The parameters are as follows; k = Boltzmann's constant, θ = absolute temperature, $\mathcal{L}^{-1}$ = inverse Langevin function given by $\mathcal{L}^{-1}(x) = \coth(x) - \frac{1}{x}$. There are numerous ways of numerically approximating the inverse Langevin function with the most common one being the Padé approximant[46] as shown in Equation (33).

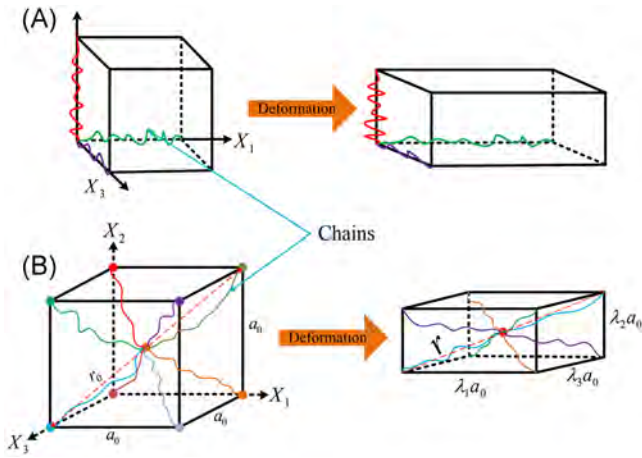$$\mathcal{L}^{-1}(x) \approx x\frac{3-x^2}{1-x^2}. \tag{33}$$

FIGURE 3 Schematic of the representative network structures for (A) three-chain and (B) eight-chain models showing both the undeformed and deformed states

To formulate a micromechanical-based constitutive model, a representative network structure is necessary to relate the chain stretch of the individual polymeric chains to the applied deformation. Various micromechanical-inspired hyperelastic models with their corresponding network structures are presented in this section.

3.1 | Three-chain model

The representative network structure of the 3-chain model[47,48] has three chains (3-chain) with each located along the axes of the undeformed cubic cell as shown in Figure 3A. When the deformation is applied, the chains will deform in an affine manner with the cubic structure with the stretch on each chain corresponding to the principal stretch value.[21] The non-Gaussian distribution is utilized in deriving the strain energy function expression for the 3-chain model as shown in Equation (34).[39]

$$\Psi_{3\text{-chain}} = \frac{\mu\sqrt{N}}{3} \sum_{i=1}^{3}\left(\lambda_i\beta_i + \sqrt{N}\ln\left(\frac{\beta_i}{\sinh\beta_i}\right)\right), \quad (34)$$

where λ_i = principle stretch in the ith axis, $\beta_i = \mathcal{L}^{-1}\left(\frac{\lambda}{\sqrt{N}}\right)$, and N = the total number of chains in the three principal directions.

The stress–stretch expressions for the three loading modes when incompressibility is considered according to Steinmann et al.[9] are given in Equation (35).

$$\sigma_{UT} = \frac{1}{3}\mu\left[\frac{3\lambda N - \lambda^3}{N - \lambda^2} - \lambda^{-2}\frac{3N - \lambda^{-1}}{N - \lambda^{-1}}\right],$$

$$\sigma_{ET} = \frac{1}{3}\mu\left[\frac{3\lambda N - \lambda^3}{N - \lambda^2} - \lambda^{-5}\frac{3N - \lambda^{-4}}{N - \lambda^{-4}}\right], \quad (35)$$

$$\sigma_{PS} = \frac{1}{3}\mu\left[\frac{3\lambda N - \lambda^3}{N - \lambda^2} - \lambda^{-3}\frac{3N - \lambda^{-2}}{N - \lambda^{-2}}\right].$$

The subscripts UT, ET, and PS represents the uniaxial tension, equibiaxial tension, and pure shear, respectively.

The 3-chain model requires two material parameters (μ and N) for each of the loading modes. The model's predictions compared to Treloar's data are plotted in Figure 4C. It can be observed that the model fits excellently to the uniaxial tension data but fails to capture accurately the biaxial and planar shear behavior.

3.2 | Eight-chain model

The model was developed by Arruda and Boyce,[12] thus, sometimes referred to as the Arruda-Boyce model. Its representative network structure has EC (hence the name 8-chain model) that are positioned on the diagonals of a unit cubic cell from the center of the cell to the corners.[13] As shown in Figure 3B, the side lengths of the undeformed cell and the length of the undeformed chain are taken as a_0 and r_0, respectively. A simple geometric analysis of the undeformed cube shows that $r_0 = a_0\sqrt{3}$. When the deformation is applied and the cell assumes a deformed shape, the chains deform with the cell and the resulting principle distortional stretches are denoted as λ_1^*, λ_2^*, and λ_3^*. Again from basic geometric analysis, the effective distortional chain length is obtained as $r = a_0\sqrt{(\lambda_1^*)^2 + (\lambda_2^*)^2 + (\lambda_3^*)^2}$. The effective distortional chain stretch is obtained as r/r_0 and has the expression given in Equation (36).

$$\overline{\lambda}^* = \sqrt{\frac{(\lambda_1^*)^2 + (\lambda_2^*)^2 + (\lambda_3^*)^2}{3}} = \sqrt{\frac{tr\mathbf{B}^*}{3}} = \sqrt{\frac{I_1^*}{3}}. \quad (36)$$

The stored energy function for the 8-chain model is dependent on the effective distortional stretch and is expressed as shown in Equation (37).

$$\Psi_{8\text{-chain}} = \mu\sqrt{N}\left[\beta\overline{\lambda}^* + \sqrt{N}\ln\left(\frac{\beta}{\sinh\beta}\right)\right] \quad (37)$$

where $\beta = \mathcal{L}^{-1}\left(\frac{\overline{\lambda}^*}{\sqrt{N}}\right)$.

The arbitrary loading Cauchy stress expression for the 8-chain model considering compressibility according to Bergström[32] is shown in Equation (38).

$$\sigma = \frac{\mu}{J\overline{\lambda}^*}\frac{\mathcal{L}^{-1}\left(\frac{\overline{\lambda}^*}{\lambda^{\text{lock}}}\right)}{\mathcal{L}^{-1}\left(\frac{1}{\lambda^{\text{lock}}}\right)}\mathbf{dev}[\mathbf{B}^*] + k[J - 1]\mathbf{I}. \quad (38)$$

The parameter λ^{lock} = the fully extended stretch of the chain (limiting chain stretch). Three material parameters are required which are μ, λ^{lock} and k. Assuming that the material is incompressible, only two material properties will be required (bulk modulus not needed)
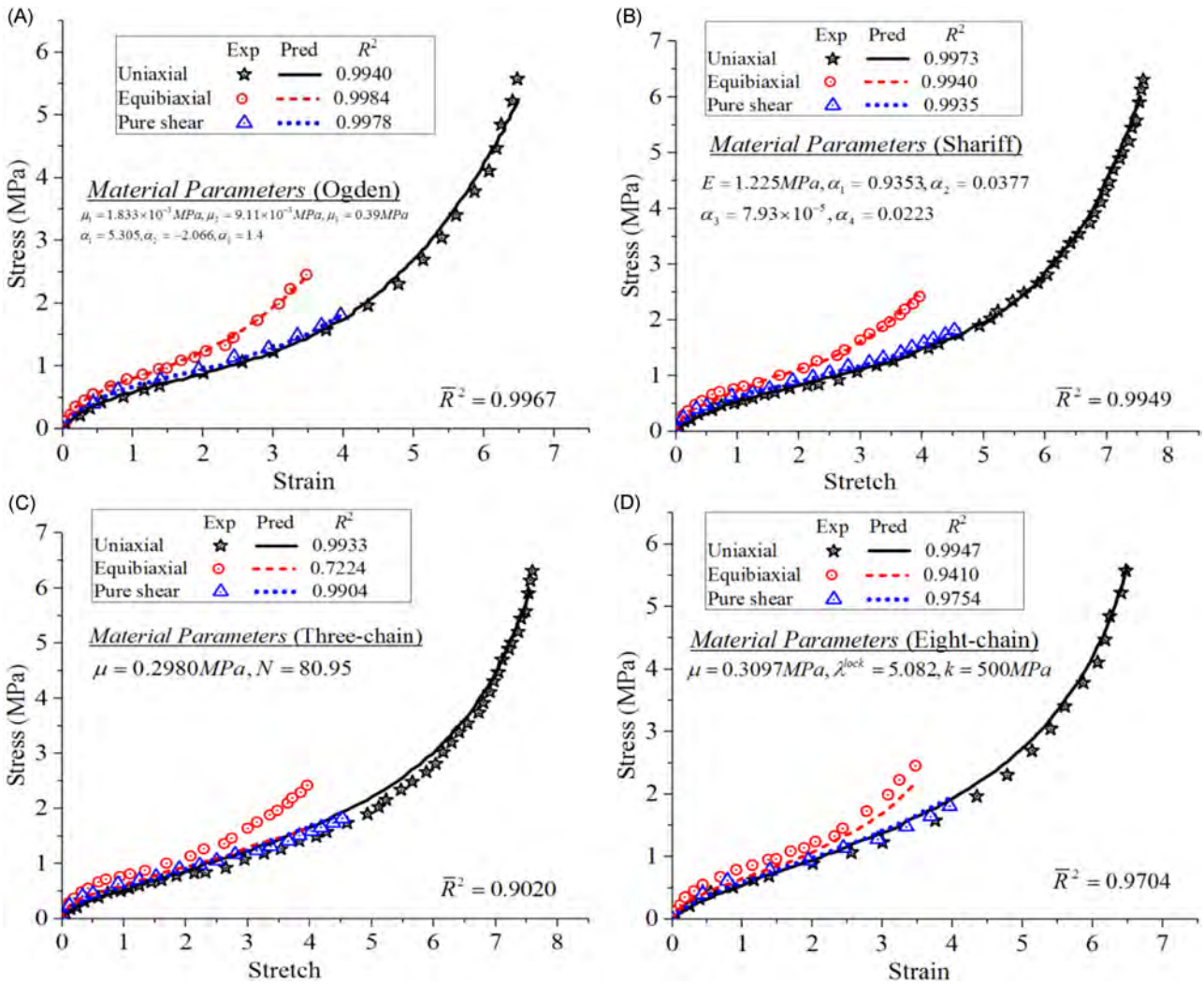
FIGURE 4 Plots of model predictions and the experimental data in three loading modes for models (A) Ogden, (B) Shariff, (C) three-chain, and (D) eight-chain

and the Cauchy stress expressions for the three loading modes are given in Equation (39).

$$\sigma_{UT} = \frac{\mu}{\overline{\lambda}^*} \frac{\mathcal{L}^{-1}\left(\frac{\overline{\lambda}^*}{\lambda^{lock}}\right)}{\mathcal{L}^{-1}\left(\frac{1}{\lambda^{lock}}\right)}\left[\lambda^2 - \frac{1}{\lambda}\right],$$

$$\sigma_{PS} = \frac{\mu}{\overline{\lambda}^*} \frac{\mathcal{L}^{-1}\left(\frac{\overline{\lambda}^*}{\lambda^{lock}}\right)}{\mathcal{L}^{-1}\left(\frac{1}{\lambda^{lock}}\right)}\left[\lambda^2 - \frac{1}{\lambda^2}\right],$$

$$\sigma_{ET} = \frac{\mu}{\overline{\lambda}^*} \frac{\mathcal{L}^{-1}\left(\frac{\overline{\lambda}^*}{\lambda^{lock}}\right)}{\mathcal{L}^{-1}\left(\frac{1}{\lambda^{lock}}\right)}\left[\lambda^2 - \frac{1}{\lambda^4}\right]. \tag{39}$$

The prediction of the 8-chain model is plotted against the experimental results of Treloar in Figure 4D. Since it is independent of the second invariant, the accuracy of the biaxial loading prediction is low. Nonetheless, the model is observed to be more accurate than some of the phenomenological models such as Mooney–Rivlin.

3.3 | Tube model

Based on the notion that the microstructure of a rubber-like material comprises highly entangled polymer chains, Heinrich and Kaliske[49] formulated a hyperelastic model in which the polymeric chains are assumed to be constrained in a tube formed by the surrounding chains.[10] When the deformation is applied, the chains in the tube are assumed to deform proportionately to the macroscopic network. Derivation of the strain energy density function, as with any other macromechanical model, is based on the statistical mechanics of polymer chains and is composed of two parts as shown in Equation (40). The first and the second parts represent the contribution from the chain cross-linking and the chain entanglement respectively.

$$\Psi = \sum_{i=1}^{3} \frac{G_c}{2}(\lambda_i^2 - 1) + \frac{2G_e}{\beta^2}(\lambda_i^{-\beta} - 1). \tag{40}$$

The terms G_c, G_e and β in Equation (40) above are the material parameters required for the tube model where $0 < \beta \leq 1$. The subscripts c and e represent the chain cross-linking and entanglement, respectively. It is worth noting that if $\mu_1 = G_c$, $\mu_2 = \frac{-2G_e}{\beta^2}$, $\alpha_1 = 2$, and $\alpha_2 = \beta$, then the tube model becomes equivalent to the second term Ogden model discussed in Section 2.2.2.

According to Hossain and Steinmann,[43] the stress expressions for uniaxial tension, equibiaxial tension, and planar shear loading modes considering incompressibility are given in Equation (41).

$$\sigma_{UT} = G_c\left[\lambda - \frac{1}{\lambda^2}\right] + \frac{2G_e}{\beta}\left[\lambda^{\frac{\beta}{2}-1} - \lambda^{-\beta-1}\right],$$

$$\sigma_{EB} = G_c\left[\lambda - \frac{1}{\lambda^5}\right] + \frac{2G_e}{\beta}[\lambda^{2\beta-1} - \lambda^{-\beta-1}], \quad (41)$$

$$\sigma_{PS} = G_c\left[\lambda - \frac{1}{\lambda^3}\right] + \frac{2G_e}{\beta}[\lambda^{\beta-1} - \lambda^{-\beta-1}].$$

A comparison of the tube's model predictions to the experimental results by Treloar is plotted in Figure 5A. The model cannot satisfactorily predict the material's behavior. It is mentioned[43] that the reason is that the energy contribution from the chain cross-linking is of NH type and, therefore, the S-shaped curve which is synonymous with rubber-like materials from moderate to high stretch values cannot be realized by the model.

3.4 | Extended tube model

The same authors of the tube model, Kaliske and Heinrich,[50] sought to improve the predictive ability of the tube model especially at moderate to high deformations by replacing the Gaussian distribution with the non-Gaussian one on the strain energy density contribution of the chain cross-linking. They added an extra inextensibility parameter δ to the chain cross-link part of the strain energy expression while maintaining the entanglement part as in the tube model. Considering that the material is compressible, a third part is added to the strain energy function which is
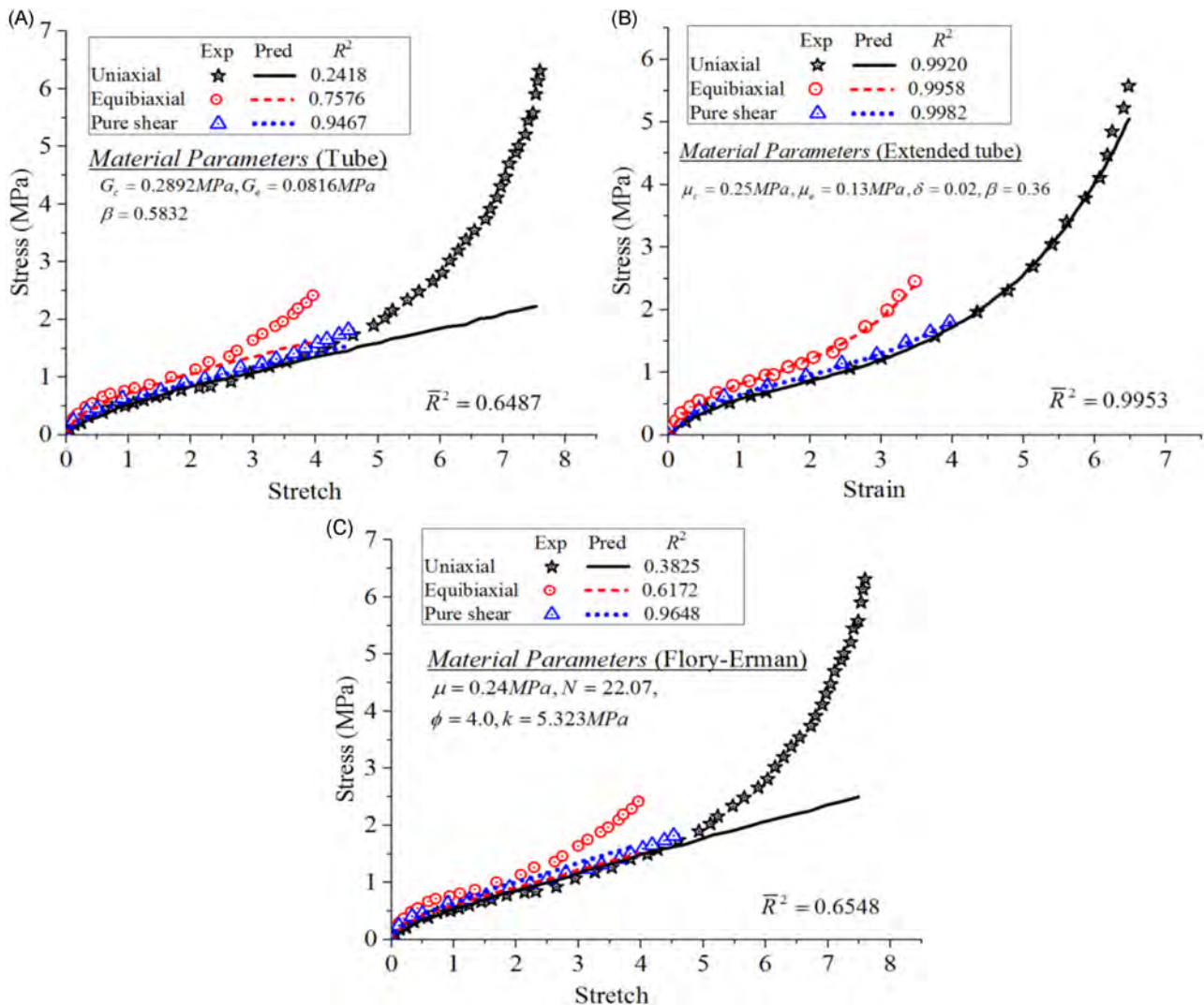

FIGURE 5 Comparisons of model predictions and the experimental data for models (A) tube, (B) extended tube, and (C) Flory–Erman

the energy from the volumetric deformations.[32] The new strain energy function has three parts as shown in Equation (42).

$$\Psi = \frac{\mu_c}{2}\left[\frac{[1 - \delta^2][I_1 - 3]}{1 - \delta^2[I_1 - 3]} + \ln(1 - \delta^2[I_1 - 3])\right] + \sum_{i=1}^{3}\frac{2\mu_e}{\beta^2}[\lambda_i^{-\beta} - 1]$$
$$+ k(J - 1)^2. \tag{42}$$

There are five material parameters required for the compressible version of the extended tube model as observed in its strain energy function namely μ_c, μ_e, δ, k, and $\beta(0 < \beta \leq 1)$. As the chains fully stretch at large deformations, the energy contribution from the entanglement part becomes insignificant. The Cauchy stress expression for the compression version of the extended tube model as given by Bergström[32] is shown in Equation (43).

$$\sigma = \frac{\mu_c}{J}\left\{\frac{1 + (1 + (I_1^*) - 4I_1^*)\delta^2 + (5I_1^* - (I_1^*) - 6)\delta^4}{[1 - (I_1^* - 3)\delta^2]^2}\right\}dev[\mathbf{B}^*]$$
$$- \frac{2\mu_e}{J\beta}\sum_{i=1}^{3}\left[(\lambda_i^*)^{-\beta} - \frac{1}{3}((\lambda_1^*)^{-\beta} + (\lambda_2^*)^{-\beta} + (\lambda_3^*)^{-\beta})\right]\hat{n}_i \otimes \hat{n}_i + k(J - 1)\mathbf{I} \tag{43}$$

where $\lambda_i^* = J^{-1/3}\lambda_i$ and the other terms remain as previously defined.

According to Hossain and Steinmann,[43] the stress expressions derived from the strain energy density function for the three loading modes considering incompressibility are given in Equation (44).

$$\sigma_{UT} = \mu_c\left[\lambda - \frac{1}{\lambda^2}\right]\left[\frac{1 - \delta^2}{[1 - \delta^2[I_1^* - 3]]^2} - \frac{\delta^2}{[1 - \delta^2[I_1^* - 3]]}\right]$$
$$+ \frac{2\mu_e}{\beta}\left[\lambda^{\frac{\beta}{2}-1} - \lambda^{-\beta-1}\right],$$

$$\sigma_{EB} = \mu_c\left[\lambda - \frac{1}{\lambda^5}\right]\left[\frac{1 - \delta^2}{[1 - \delta^2[I_1^* - 3]]^2} - \frac{\delta^2}{[1 - \delta^2[I_1^* - 3]]}\right]$$
$$+ \frac{2\mu_e}{\beta}[\lambda^{2\beta-1} - \lambda^{-\beta-1}], \tag{44}$$

$$\sigma_{PS} = \mu_c\left[\lambda - \frac{1}{\lambda^3}\right]\left[\frac{1 - \delta^2}{[1 - \delta^2[I_1^* - 3]]^2} - \frac{\delta^2}{[1 - \delta^2[I_1^* - 3]]}\right]$$
$$+ \frac{2\mu_e}{\beta}[\lambda^{\beta-1} - \lambda^{-\beta-1}].$$

The extended tube model's predictions fit the experimental Treloar data to a very high level of accuracy as shown in Figure 5B. The extended tube model is one of the most accurate hyperelastic material models. The material parameters for uniaxial loading mode can be used to predict the behavior of other loading modes.

3.5 | Flory–Erman

The Flory and Erman model[51] begins by assuming that the strain energy density of a polymer network exhibiting high elasticity is expressed as a sum of two contributions. The first contribution is from the phantom network (defined as a network whereby the physical effects of the chains between junctions are confined entirely to the forces they exert on the pairs of the junctions to which each is attached) whereas the

second contribution is from the constraints emerging from the material properties of chains that are densely distributed in a random network (see Equation 45).

$$\Psi = \Psi_{ph} + \Psi_{ct}. \tag{45}$$

The subscripts ph and ct represent phantom and constraint, respectively. Furthermore, the phantom network energy is derived from the Gaussian chain statistics hence equivalent to the neo-Hookean strain energy density as shown in Equation (46) according to Hossain and Steinmann.[43]

$$\Psi_{ph} = \sum_{i=1}^{3}\frac{\mu}{2}\left[1 - \frac{1}{\varphi}\right]\left[\lambda_i^2 - 1\right]. \tag{46}$$

The parameter φ in Equation (46) represents the number of chains at a junction whereas μ is the shear modulus. On the other hand, the expression for the constraint contribution of the strain energy is derived from the micromechanics of the chain molecules as is given in Equation (47).

$$\Psi_{ct} = \sum_{i=1}^{3}\frac{\mu}{2}[B_i + D_i - \ln(B_i + 1) - \ln(D_i + 1)], \tag{47}$$

where $B_i = k^2[\lambda_i^2 - 1][\lambda_i^2 + k]^{-2}, D_i = \lambda_i^2 k^{-1}B_i$. The parameter k represents the strengths of the constraints. Considering incompressibility, the stress-stretch relationship expressions for the three deformation modes are given in Equation (48).

$$\sigma^{UT} = \mu\left[1 - \frac{2}{\varphi}\right]\left[\lambda - \frac{1}{\lambda^2}\right] + \sigma_{ct}^{UT},$$

$$\sigma^{EB} = \mu\left[1 - \frac{2}{\varphi}\right]\left[\lambda - \frac{1}{\lambda^5}\right] + \sigma_{ct}^{EB}, \tag{48}$$

$$\sigma^{PS} = \mu\left[1 - \frac{2}{\varphi}\right]\left[\lambda - \frac{1}{\lambda^3}\right] + \sigma_{ct}^{PS},$$

where the subscript ct represents the stress contribution from the constraints and is obtained by differentiating the constraints part of the strain energy density function expression given in Equation (47). The material behavior predictions of the Flory–Erman model compared to the experimental data of Treloar are plotted in Figure 5C. The model makes reasonable predictions up to moderate stretches but significant deviations from the experimental S-shaped curved at high stretches are encountered. This is because of the assumptions of the Gaussian statistics on the Phantom part of the strain energy density function.

4 | PREDICTIVE PERFORMANCE OF THE MODELS

As numerical simulations are increasingly becoming an integral part of engineering components design, design engineers are constantly faced with the challenge of choosing the right hyperelastic

constitutive model since it is a crucial prerequisite for good numerical predictions. It is, therefore, imperative to present how each of the models reviewed in this study performs in their predictions. There is no clearly defined method of ranking the models and, therefore, researchers have employed varying methods. Marckmann and Verron[10] ranked 20 hyperelastic models based on their abilities to reproduce two sets of experimental data by Treloar[11] and Kawabata et al.[52] The models that could predict accurately the three modes of loading in the two sets of data were considered as the best whereas those that required a higher number of material parameters were ranked lowly. Badienia,[39] utilized the quality of fit measure whereby the models that reproduced the S-shaped curve of the Treloar's experimental data stress-stretch plot to a higher level of fit were ranked highly. Using Treloar's data, Bergström[32] ranked the models based on the coefficient of determination and also the number of material parameters required. Applying a slightly different approach, Ritto and Nunes[53] utilized two methods in ranking five hyperelastic materials. First, they ranked according to the error between the predicted and the experimental data considering two loading modes; pure and simple shear. Second, they developed a model based on Bayesian statistics which they found to be comprehensive in ranking a given set of hyperelastic models.

In general, two factors are crucial in determining a model's rank. The first and most important factor is the model's capability in replicating the experimental data in all of the three modes of loading namely uniaxial tension, equibiaxial tension, and pure shear. The second is the number of material parameters required by the model. This influences in that a higher number of parameters means more tedious experimental work is required to calibrate the model. This may not be much of an issue these days since codes that accurately approximate the material parameters for hyperelastic models based on uniaxial loading data have been developed such as the MCalibration.[54] In this section, we will present the predictive performances of the hyperelastic models on each of the three loading modes based on the coefficient of determination. Finally, we will propose a new ranking method that is based on the ability of the model to accurately predict the behavior in the three loading modes taking into account the deviation of the R^2 values. Based on our observation, some models are excellent in predicting the behavior in one mode, for example, uniaxial tension but poorly predict the other modes of loading. We propose that a good model should be able to predict all three modes accurately with minimum differences in the R^2 values.

4.1 | Uniaxial tension

As shown in Figure 6, the majority of the models discussed predict the uniaxial tension behavior accurately with R^2 values of over 0.98. On the other hand, the Valanis–Landel model performs extremely poorly in predicting uniaxial behavior with R^2 value of about 0.1. The 3-chain, EC, HS, and Gent exhibit excellent predicted results while requiring only three material parameters hence can be rated as top-performing models for uniaxial tension prediction.
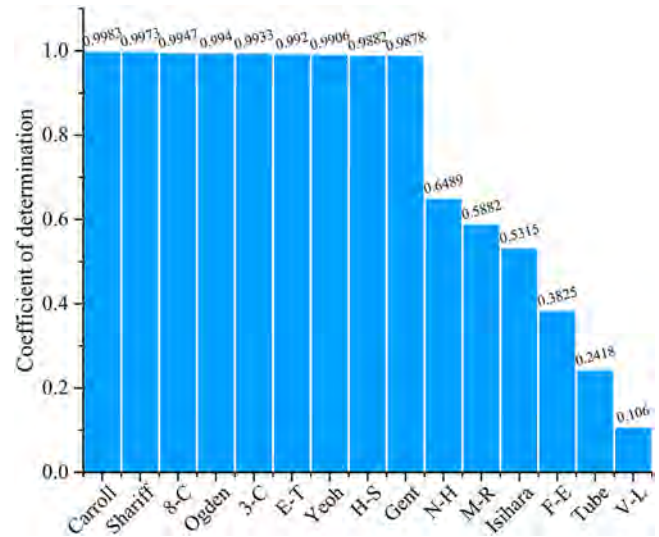

FIGURE 6 Performance of the models in uniaxial tension loading based on R^2 values

4.2 | Equibiaxial tension

The performance of the models in the equibiaxial tension is better than in the uniaxial tension as shown in Figure 7. Even though the Ogden model's predictions agree excellently with the observed experimental behavior as demonstrated by the R^2 of 0.9984, it requires seven material parameters hence models such as Mooney–Rivlin and EC are preferred since they require only three parameters and exhibits almost similar accuracy levels. Again, the Valanis–Landel model poorly predicts the equibiaxial loading but better than in the uniaxial tension.

4.3 | Pure shear

All the models reviewed in this study predict the planar shear loading behavior pretty accurately. As shown in Figure 8, the highest and the lowest R^2 values are 0.9982 and 0.8664 for the extended tube and the Valanis–Landel models, respectively. With only three parameters, the 3-chain, EC, Horgan-Saccomandi, and Gent models are the best choices for this loading type since their predictions agree with over 97% of the experimental data.

4.4 | Overall predictive capabilities

To deduce the $\bar{R}^2$ value for the overall predictive capability for each of the models, a simple average of the R^2 values for the three loading modes was obtained. Without considering the number of material parameters required, the Ogden, Carroll, Extended tube, and Shariff models are the best with over 0.99 $\bar{R}^2$ values as shown in Figure 9.
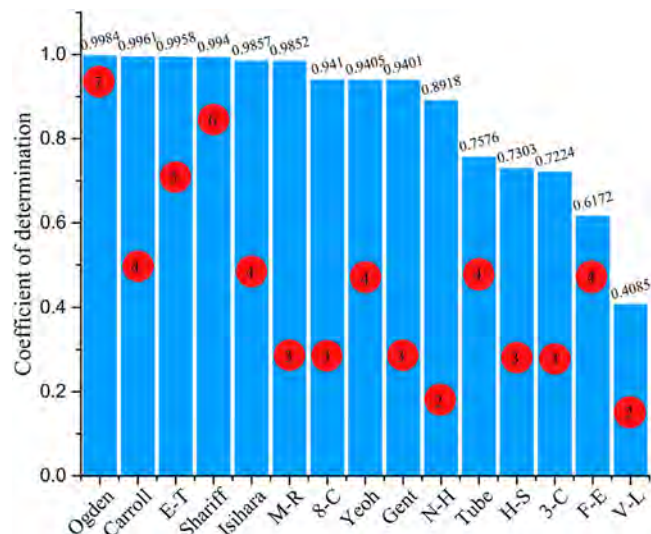
FIGURE 7 Performance of the models in equibiaxial tension loading. The number of material parameters in each model is shown in red circles
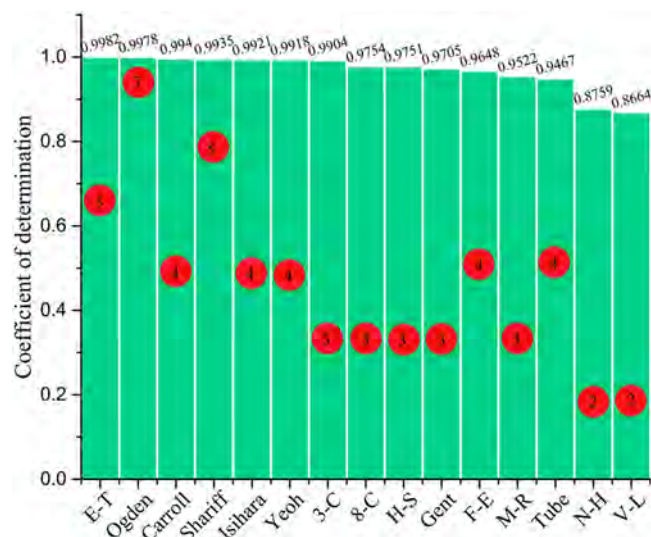

FIGURE 9 Overall predictive performances of the models

FIGURE 8 Predictive performance of the models in pure shear loading

4.5 | Proposed ranking method

Indeed, understanding the best model to use in designing hyperelastic-based components is crucial for the success of the design process. As such, ranking of hyperelastic models is an important part of a review work yet very few authors in the literature have addressed it. To the best of our knowledge, Marckmann and Verron[10] were the first authors to propose a ranking scheme that was mainly based on the ability of the model to achieve complete behavior, that is, reproduce experimental data in different types of loading conditions. They also considered the number of material parameters and whether the model is micromechanical or phenomenological. The
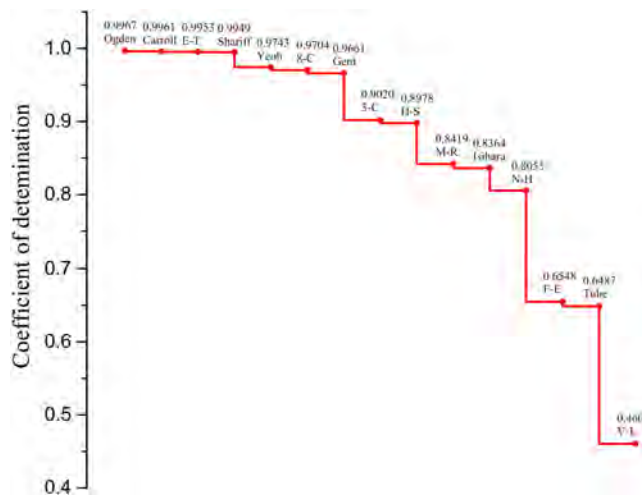
recent work by Dal et al.[22,23] based their ranking on quality of fit for simultaneous fits. Generally, the overall behavior is quantified by obtaining the average of the quality of fit in all the loading modes. This may be inaccurate in some cases. For instance, a model with high and low accuracies in two different loading modes may still record a higher average (overall) behavior than a model with acceptable accuracies in all loading modes. Therefore, a more accurate ranking system must consider the deviations in the quality of fit in individual loading modes. While the number of parameters of a highly ranked model should be as few as possible, it should have little influence on the ranking as the modern computational capabilities of computers are highly advanced and some algorithms easily determine the parameters for phenomenological models. In the case of two models with the same predictive performance, the one with fewer parameters will be preferred and ranked higher.

In this section, we propose a ranking scheme based on two important functions of the models and without considering the number of material parameters required. First, the model should not only be able to reproduce the experimental data in the three loading modes to a higher level of accuracy but should also have minimum deviations (found by calculating the SD) between the R^2 values for each of the loading modes. This means that a model with high predictive capability in one loading mode and low in the other will be ranked low. Second, the $\bar{R}^2$ value is taken into consideration by categorizing those that fall between 0.95-1.0 as index 1, 0.90-0.94 as index 2, 0.85-0.89 as index 3, and so on. The ranking coefficient will be the sum of the SD and the index value of the model. The model with the lowest ranking coefficient (meaning both the SD and the index value are the lowest) is taken as the best. The summary of the ranking is presented in Table 1 below. The best-ranked models from the scheme include the Shariff, Carroll, Ogden, extended tube, Gent, and EC. On the other hand, the poorly ranked models include the Valanis–Landel, tube, and the Flory–Erman. While we believe that the ranking scheme introduced can be reliable in determining the best models for material behavior prediction, it is worth noting that it was introduced specifically for this review work and is not intended to be an authoritative

TABLE 1 Ranking of the hyperelastic models

Rank	Model	Coefficient of determination				SD	Range	Index	Ranking coefficient
		UT	EB	PS	Overall				
1	Shariff	0.9973	0.994	0.9935	0.9949	0.001685	0.95–1.0	1	1.001685
2	Carroll	0.9983	0.9961	0.9940	0.9961	0.001755	0.95–1.0	1	1.001755
3	Ogden	0.994	0.9984	0.9978	0.9967	0.001948	0.95–1.0	1	1.001948
4	ET	0.992	0.9958	0.9982	0.9953	0.002552	0.95–1.0	1	1.002552
5	Gent	0.9878	0.9401	0.9705	0.9661	0.019716	0.95–1.0	1	1.019716
6	E-C	0.9947	0.941	0.9754	0.9704	0.022209	0.95–1.0	1	1.022209
7	Yeoh	0.9906	0.9405	0.9918	0.9743	0.023905	0.95–1.0	1	1.023905
8	3-C	0.9933	0.7224	0.9904	0.9020	0.127025	0.90–0.94	2	2.127025
9	HS	0.9882	0.7303	0.9751	0.8978	0.118586	0.85–0.89	3	3.118586
10	N-H	0.6489	0.8918	0.8759	0.8055	0.110946	0.80–0.84	4	4.110946
11	M-R	0.5882	0.9852	0.9522	0.8419	0.179874	0.80–0.84	4	4.179874
12	Isihara	0.5315	0.9857	0.9921	0.8364	0.215636	0.80–0.84	4	4.215636
13	F-E	0.3825	0.6172	0.9648	0.6548	0.239207	0.65–0.69	7	7.239207
14	Tube	0.2418	0.7576	0.9467	0.6487	0.297898	0.60–0.64	8	8.297898
15	V-L	0.106	0.4085	0.8664	0.4601	0.312585	0.45–0.49	11	11.31258

Note: ET, E-C, HS, 3-C, N-H, M-R, F-E, and V-L represents extended tube, eight-chain, Horgan-Saccomandi, three-chain, Neo-Hookean, Mooney-Rivlin, Flory-Erman, and Valanis-Landel respectively. The UT, EB, and PS represent uniaxial tension, equibiaxial tension, and pure shear, respectively.

guide in choosing hyperelastic models. Since the Shariff and the Carroll models are not available in most of the finite element codes, Ogden, EC, and neo-Hookean models remain the most commonly used because of their availability.

5 | RELEVANCE TO MECHANICAL SYSTEM DYNAMICS

One of the main topics in mechanical system dynamics is in modeling and computation where formulation of finite element system dynamics with characteristics such as large deformation and non-linearity is undertaken. These simulations are nowadays a requisite part of the product design process in addition to physical experiments. The success of such formulations in terms of accuracy and reliability of the simulation results depends on accurate constitutive relations that describe mechanical behavior with the mentioned characteristics. Therefore, knowledge of hyperelastic models is highly relevant to the advancement of mechanical system dynamics.

Vibration control and damping are highly relevant in mechanical system dynamics. Mechanical systems exhibit vibrations (when subjected to loading conditions) which are undesirable in many engineering applications as they may lead to damaging effects on the system. Besides being highly nonlinear elastic and capable of undergoing large deformations, elastomeric materials exhibit viscous behavior i.e. high damping and energy storage capabilities. Consequently, they are widely utilized in fabricating shock absorbers that reduce the vibrations and shock loadings

in dynamic mechanical systems. To predict the system behavior, two kinds of constitutive models are necessary; hyperelastic and viscoelastic models. The former is responsible for predicting the large nonlinear elastic behavior whereas the latter predicts the time-dependent response. This study contributes to the understanding of hyperelastic behavior which is indispensable in vibration control and damping in mechanical system dynamics.

6 | CONCLUSIONS

Hyperelastic materials are so-called because, intrinsically, they can undergo finite deformations that can be completely recovered upon removal of the load and the material resumes its initial state, that is, no internal energy dissipation. It constitutes a large number of important engineering materials such as elastomers, polymers, and soft tissues. Developing the constitutive models for these materials begins with defining the expression for an energy potential known by names such as Helmholtz free energy per unit reference volume, strain energy density, or elastic potential. There are two main approaches to formulating the elastic potential; the micromechanical and the phenomenological approach. The former involves the utilization of statistical mechanics theories on the networks formed by polymeric chains at the microstructure level of the material and are sometimes known as statistical approaches whereas the latter involves the fitting of mathematical equations to the experimental data. The stress–strain or stress–stretch behavior of the hyperelastic material is then obtained by the derivative of the elastic

potential with respect to the strain invariants or the principal stretches. The material is assumed to be homogenous and isotropic. Incompressibility is mostly assumed to simplify the stress–strain expressions.

For the interest of research and design engineers, this study employed a unique approach to bring about the knowledge of constitutive models for large nonlinear elastic mechanical behavior of elastomeric materials in a succinct manner. The models were categorized based on the approach in which the strain energy density expression is formulated, phenomenological or micromechanical. The former was further grouped into those that are dependent on the strain invariants of the Cauchy–Green deformation tensors or principal stretches. For each model, emphasis was placed on the strain energy density expression, the stress–strain or stress–stretch expression for arbitrary or specific loading conditions, and the material parameters for the classical Treloar's experimental data. Importantly, the predictive performances of the models were ascertained by comparing the predicted stress–stretch or stress–strain data to the experimental data by Treloar where the coefficient of determination (R^2) was employed to determine the closeness of the predicted and the experimental data. The predictive performance was presented in two ways; first for each loading mode (uniaxial tension, equibiaxial extension, and pure shear) and second for the overall or complete behavior in which the average of the coefficient of determination in each loading mode was utilized. Since the performance of the models in different loading modes varies, it is important to establish both the individual and overall behavior. Except for the single-parameter models with a linear dependence on the first invariant, the predictive performance in the uniaxial tension and pure shear was to an acceptable accuracy level. On the other hand, the equibiaxial loading proved to be the most difficult to reproduce by most models. An excellent model that can be utilized to predict the practical behavior of complex 3D components under arbitrary loading conditions should reproduce the experimental data in all the loading modes accurately. Furthermore, a model with a minimum number of material parameters is highly desirable as more will mean increased complexity of the model and the calibration process may lead to instabilities in the parameters. This study proposed a ranking method whereby the model with a high $\bar{R}^2$ value (the average of the R^2 values for the three loading modes) and minimum deviations between the R^2 values for each of the loading modes, is considered as the best.

As the computational capabilities of modern computers continue to soar high, the numerical simulations via finite element codes increasingly become indispensable in the component design process and so is the development of the constitutive models. While it is highly encouraged to have models with fewer material parameters for simplicity, stability, and low computational costs, what will matter in the future is the ability of the model to accurately predict the material behavior under arbitrary loading as there are algorithms that extract material parameters from simple uniaxial loading data. On top of achieving models that accurately describe the experimental behavior in all kinds of loading conditions, future research should focus on addressing some of the main drawbacks of the current models that include the number of experimental data required for calibrating phenomenological models and the range of applicability of the

models. For stable parameters, the majority of the models require simultaneous fitting to both uniaxial tension and equibiaxial extension data. This is disadvantageous since it increases the number of experiments, the time, and the cost of calibrating models. Furthermore, the equibiaxial loading experimental setup is complicated and prone to errors. On the range of applicability, some models are accurate but only to a limited strain range, for example, moderate strains. Researchers should strive to achieve models that work in the full strain range.

CONFLICT OF INTEREST

The authors declare that there are no conflict of interest.

AUTHOR CONTRIBUTIONS

Stephen K. Melly: Conceptualization, methodology, software, formal analysis, data curation, writing—original draft. **Liwu Liu**: Conceptualization, methodology, validation, writing—review and editing. **Yanju Liu**: Conceptualization, methodology, validation, writing—review and editing. **Jinsong Leng**: Writing—review and editing, resources, supervision, funding acquisition.

DATA AVAILABILITY STATEMENT

The data that support the findings of this study are available from the corresponding author upon reasonable request.

ORCID

Stephen K. Melly http://orcid.org/0000-0001-9253-2271
Jinsong Leng http://orcid.org/0000-0001-5098-9871

REFERENCES

1. Ramezani M, Ripin ZM. Characteristics of elastomer materials. *Rubber-Pad Forming Processes*. Woodhead Publishing; 2012.
2. Ali A, Hosseini M, Sahari BB. A review of constitutive models for rubber-like. *Mater Am J Eng Appl Sci*. 2010;3(1):232-239.
3. Mooney M. A theory of large elastic deformation. *J Appl Phys*. 1940; 11(9):582-592.
4. Chaves EWV. *Hyperelasticity*. Notes on Continuum Mechanics. 1st ed. Springer; 2013.
5. Ward IM, Sweeney J. The behaviour in the rubber-like state: Finite strain elasticity. *Mechanical Properties of Solid Polymers*. John Wiley & Sons, Ltd; 2012.
6. Ruíz MJG, González LYS. Comparison of hyperelastic material models in the analysis of fabrics. *Int J Clothing Sci Technol*. 2006;18(5):314-325.
7. Ogden RW. *Elasticity*. Non-Linear Elastic Deformations. Dover Publications; 1997.
8. Bahreman M, Darijani H, Fooladi M. Constitutive modeling of isotropic hyperelastic materials using proposed phenomenological models in terms of strain invariants. *Polym Eng Sci*. 2016;56(3):299-308.
9. Steinmann P, Hossain M, Possart G. Hyperelastic models for rubber-like materials: consistent tangent operators and suitability for Treloar's data. *Arch Appl Mech*. 2012;82:1183-1217.
10. Marckmann G, Verron E. Comparison of hyperelastic models for rubber-like materials. *Rubber Chem Technol*. 2006;79(5):835-858.

11. Treloar LRG. Stress-strain data for vulcanized rubber under various types of deformation. *Rubber Chem Technol*. 1944;17(4):813-825.

12. Arruda EM, Boyce MC. A three-dimensional constitutive model for the large stretch behavior of rubber elastic materials. *J Mech Phys Solids*. 1993;4(2):389-412.

13. Hossain M, Amin AFMS, Kabir MN. Eight-chain and full-network models and their modified versions for rubber hyper-elasticity: a comparative study. *J Mech Behav Mater*. 2015;24(1-2):11-24.

14. Miroshnychenko D, Green WA. Heuristic search for a predictive strain-energy function in nonlinear elasticity. *Int J Solids Struct*. 2009;46(2):271-286.

15. Melly SK, Liu L, Liu Y, Leng J. Improved Carroll's hyperelastic model considering compressibility and its finite element implementation. *Acta Mech Sinica*. 2021;37:785-796.

16. Carroll MM. A strain energy function for vulcanized rubbers. *J Elast*. 2011;103:173-187.

17. Anssari-Benam A, Bucchi A. A generalised neo-Hookean strain energy function for application to the finite deformation of elastomers. *Int J Non Linear Mech*. 2021;128:103626.

18. Martins Pals JRMN, Ferreira AJM. A comparative study of several material models for prediction of hyperelastic properties: application to silicone-rubber and soft tissues. *Strain*. 2006; 42(3):135-147.

19. Martins JAC, Pires EB, Salvado R, Dinis PB. PB. A numerical model of passive and active behavior of skeletal muscles. *Comput Methods Appl Mech Energy*. 1998;151:419-433.

20. Sweeney J. A comparison of three polymer network models in current use. *Comput Theor Polym Sci*. 1999;9:27-33.

21. Boyce MC, Arruda EM. Constitutive models of rubber elasticity: a review. *Rubber Chem Technol*. 2000;73(3):504-523.

22. Dal H, Badienia Y, Açikgöz K, Denlï FA. A comparative study on hyperelastic constitutive models on rubber: State of the art after 2006. In: Huneau B, Cam JBL, Marco Y, Verron E, eds. *Constitutive Models for Rubber XI*. 1st ed. CRC Press; 2019.

23. Dal H, Açıkgöz K, Badienia Y. On the performance of isotropic hyperelastic constitutive models for rubber-like materials: a state of the art review. *Appl Mech Rev*. 2021;73(2):020802.

24. Vahapoğlu V, Karadeniz S. Constitutive equations for isotropic rubber-like materials using phenomenological approach: a bibliography (1930–2003). *Rubber Chem Technol*. 2006;79(3):489-499.

25. Mansouri MR, Darijani H. Constitutive modeling of isotropic hyperelastic materials in an exponential framework using a self-contained approach. *Int J Solids Struct*. 2014;51:4316-4326.

26. Rivlin RS. Large elastic deformations of isotropic materials. I. Fundamental concepts. *Phil Trans R Soc London A, Math Phys Sci*. 1948; 240(822):459-490.

27. Valanis KC, Landel RF. The strain-energy function of a hyperelastic material in terms of the extension ratios. *J Appl Phys*. 1967;38(7): 2997-3002.

28. Ogden RW. Large deformation isotropic elasticity—on the correlation of theory and experiment for incompressible rubberlike solids. *Proc R Soc Lond A*. 1972;326(1567):565-584.

29. Beda T. An approach for hyperelastic model-building and parameters estimation a review of constitutive models. *Eur Polym J*. 2014;50:97-108.

30. Horgan CO, Murphy JG. On the volumetric part of strain-energy functions used in the constitutive modeling of slightly compressible solid rubbers. *Int J Solids Struct*. 2009;46:3078-3085.

31. González DG. *A continuum mechanics framework for hyperelastic materials: connecting experiments and modelling*. Doctoral dissertation. University Carlos III of Madrid; 2016.

32. Bergström J. Mechanics of solid. *Polymers: Theory and Computational Modeling*. William Andrew; 2015.

33. Yeoh OH. Characterization of elastic properties of carbon-black-filled rubber vulcanizates. *Rubber Chem Technol*. 1990;63(5):792-805.

34. Yeoh OH. Some forms of the strain energy function for rubber. *Rubber Chem Technol*. 1993;66(5):754-771.

35. Kawabata S, Yamashita Y, Ooyama H, Yoshida S. Mechanism of carbon-black reinforcement of rubber vulcanizate. *Rubber Chem Technol*. 1995;68(2):311-329.

36. Rivlin RS. Large elastic deformations of isotropic materials. iv. Further developments of the general theory. *Phil Trans R Soc London A*. 1948;241:379-397.

37. Gent AN. A new constitutive relation for rubber. *Rubber Chem Technol*. 1996;69(1):59-61.

38. Isihara A, Hashitsume N, Tatibana M. Statistical theory of rubber-like elasticity. IV. (two-dimensional stretching). *J Chem Phys*. 1951;19: 1508-1512.

39. Badienia Y. *A Comparative Study of the Fitting Performance of Hyperelastic Constitutive Models*. Thesis. Middle East Technical University; 2019.

40. Horgan CO, Saccomandi G. Constitutive modelling of rubber-like and biological materials with limiting chain extensibility. *Math Mech Solids*. 2002;7(4):353-371.

41. Rivlin RS. The Valanis–Landel strain-energy function. *J Elast*. 2003; 73:291-297.

42. Shariff MHBM. Strain energy function for filled and unfilled rubber-like material. *Rubber Chem Technol*. 2000;73(1):1-18.

43. Hossain M, Steinmann P. More hyperelastic models for rubber-like materials: consistent tangent operators and comparative study. *J Mech Behav Mater*. 2013;22(1-2):27-50.

44. Erman B, Mark JE. The molecular basis of rubberlike elasticity. In: Mark JE, Eirich FR, Erman B, eds. *Science and Technology of Rubber*. Academic Press; 2005.

45. Treloar LRG. *The Physics of Rubber Elasticity*. 3rd ed. Oxford University Press; 1975.

46. Cohen A. A Padé approximant to the inverse Langevin function. *Rheol Acta*. 1991;30:270-273.

47. James HM, Guth E. Theory of the elastic properties of rubber. *J Chem Phys*. 1943;11(10):455-481.

48. Wang MC, Guth E. Statistical theory of networks of non-gaussian flexible chains. *J Chem Phys*. 1952;20(7):1144-1157.

49. Heinrich l, Kaliske M. Theoretical and numerical formulation of a molecular based constitutive tube-model of rubber elasticity. *Comput Theor Polym Sci*. 1997;7(3-4):227-241.

50. Kaliske M, Heinrich G. An extended tube-model for rubber elasticity: statistical-mechanical theory and finite element implementation. *Rubber Chem Technol*. 1999;72(4):602-632.

51. Flory PJ, Erman B. Theory of elasticity of polymer networks. *Macromolecules*. 1982;15(3):800-806.

52. Kawabata S, Matsuda M, Tei K, Kawai H. Experimental survey of the strain energy density function of isoprene rubber vulcanizate. *Macromolecules*. 1981;14(1):154-162.

53. Ritto TG, Nunes LCS. Bayesian model selection of hyperelastic models for simple and pure shear at large deformations. *Comput Struct*. 2015;156:101-109.

54. *PolymerFEM*. May 2020. https://polymerfem.com/mcalibration/